Available online at www.sciencedirect.com
SCIENCE DIRECT®
Journal of Sound and Vibration 290 (2006) 956–967
JOURNAL OF SOUND AND VIBRATION
www.elsevier.com/locate/jsvi

Near field acoustic holography (NAH) theory for cyclostationary sound field and its application

Quan Wan*, W.K. Jiang

State Key Laboratory of Vibration, Shock & Noise, Shanghai Jiaotong University, 800 Dong Chuan Road, Shanghai 200240, the People's Republic of China

Received 9 March 2004; received in revised form 20 April 2005; accepted 2 May 2005
Available online 8 August 2005

Abstract

The cyclostationary near field acoustic holography (CYNAH) technique is proposed with a view to overcome the limitations of the traditional near field acoustic holography (NAH) technique in analyzing cyclostationary sound field. Because of the modulation of such kind of sound signal, the sidebands appear in the spectrum of sound pressure. Therefore, the power of modulating wave components cannot be correctly shown by the power spectral density (PSD) of sound pressure in NAH hologram with the disturbance of sidebands. The cyclic spectrum density (CSD) of sound pressure is shown by the CYNAH hologram instead of the spectrum. The influence of sidebands can be subdued by CYNAH because of the demodulation function of the CSD. The CYNAH hologram of an alternating motor, as an instance of cyclostationary source, is obtained in an anechoic-chamber. The results of experiment show that this approach can obtain more information about cyclostationary sound field than NAH can.

1. Introduction

Since the near field acoustic holography (NAH) technique was proposed firstly in the early 1980s [1], many approaches have been achieved for the sound field reconstruction, such as spatial transformation of sound field (STSF) [2], broadband acoustical holography from intensity

*Corresponding author. Tel.: +86 21 54747441 101; fax: +86 21 54747451.
E-mail addresses: wanquan001@sjtu.edu.cn (Q. Wan), wkjiang@sjtu.edu.cn (W.K. Jiang).

0022-460X/$ - see front matter © 2005 Elsevier Ltd. All rights reserved.
doi:10.1016/j.jsv.2005.05.002

measurement (BAHIM) [3], BEM (boundary element method)-based NAH [4], etc. These approaches are used to investigate characteristics of noise sources in engineering [5–8].

The vibration and acoustic signals of some rotating machineries, such as rolling-element bearings, gears, etc, are generally cyclostationary signals with standard modulation [9–13]. The modulating wave components usually result from periodic pulse vibration, and the carrier wave components result from the free oscillation and other random disturbance. The current NAH procedures treat cyclostationary signals as if they were statistically stationary, and on the acoustic hologram of which the spectrum or power spectral density (PSD) of sound pressure is displayed generally. However, two kinds of wave components may be mixed up in the spectrum or PSD, so that a series of sidebands will appear around the spectral lines of carrier wave. The power of modulating wave components cannot be correctly shown by the NAH hologram with the disturbance of sidebands, which generally contain some useful information for fault diagnosing in many cases.

The second-order cyclic statistics theory, such as cyclic spectral density (CSD) was used to model the vibration and acoustic signals of some rotating machineries [9–13]. Some characteristics of these signals, such as modulating wave components and carrier wave components, can be obtained solely by CSD in different cyclic frequencies, which may be mixed up in PSD and cannot be shown clearly. Thus, the disturbance of sidebands can be subdued in CSD of sound signals, and the useful information concealed in the sidebands can be extracted out in some specific cyclic frequencies.

The cyclostationary near field acoustic holography (CYNAH) procedure is presented here to analyze the cyclostationary sound field by applying the CSD to STSF procedures. Instead of the PSD or spectrum, the CSD of sound pressure is displayed by the CYNAH hologram. For so many advantages of CSD in cyclostationary signal processing, the power of the useful information concealed in the sidebands can be shown clearly by the CSD distribution of CYNAH hologram if only appropriate cyclic frequencies are selected. In this way, the detailed information about cyclostationary sound field can be obtained with CYNAH more accurately than with NAH, and it is better for the CYNAH hologram able to exhibit the underlying physical concepts of the modulation mechanism present in the vibration of rotating machineries.

2. Cyclostationarity: definition and properties

2.1. Definitions

Cyclostationarity: A random signal $u(t)$ is considered as cyclostationary at the nth order if its time-domain nth order moment is a periodical function of the time t. Here, only the second-order cyclostationarity will be discussed.

Second-order cyclostationarity: The autocorrelation function of $u(t)$ is defined by

$$R_u(t,\tau) = E\big(u\big(t+\tau/2\big)u^*\big(t-\tau/2\big)\big), \tag{1}$$

where the operator $E(\cdot)$ is the statistical average, the superscript * is a conjugate operator, and τ is time-delay. The signal $u(t)$ is second-order cyclostationary if $R_u(t,\tau) = R_u(t+T,\tau)$ for all t, T is the cyclic period, and the fundamental frequency $\alpha = 1/T$ is called cyclic frequency. The

periodical function can then be expanded into Fourier series:

$$R_u(t,\tau)=\sum_{\alpha}R_u^{\alpha}(\tau)\mathrm{e}^{-\mathrm{j}2\pi\alpha t}, \tag{2}$$

where $R_u^{\alpha}(\tau)$ is defined as the cyclic autocorrelation function. For $\alpha=0$, it simplifies to the stationary autocorrelation function. The cyclic spectral density (CSD, i.e. auto-CSD) can be expressed as

$$S_{uu}^{\alpha}(f)=\int_{-\infty}^{\infty}R_u^{\alpha}(\tau)\mathrm{e}^{-\mathrm{j}2\pi f\tau}\mathrm{d}\tau. \tag{3}$$

Note that for $\alpha=0$, the PSD can be obtained.

The CSD can be also expressed as

$$S_{uu}^{\alpha}(f)=\left\langle U\left(f+\alpha/2\right)U^{*}(f-\alpha/2)\right\rangle_t, \tag{4}$$

where the operator $\langle\cdot\rangle_t$ is time-average operator, $U(f+\alpha/2)$ and $U(f-\alpha/2)$ are spectral components of $u(t)$ at frequencies $(f+\alpha/2)$ and $(f-\alpha/2)$, respectively.

Similarly, the cross-CSD of two signals $u(t)$ and $v(t)$ can be defined as

$$S_{uv}^{\alpha}(f)=\left\langle U\left(f+\alpha/2\right)V^{*}(f-\alpha/2)\right\rangle_t. \tag{5}$$

So the cross-CSD matrix of the array vectors $\mathbf{u}(t)$ and $\mathbf{v}(t)$ can be defined as

$$\mathbf{S}_{\mathbf{uv}}^{\alpha}(f)=\left\langle \mathbf{U}\left(f+\alpha/2\right)\mathbf{V}^{\mathrm{H}}(f-\alpha/2)\right\rangle_t, \tag{6}$$

where the superscript H is conjugate-transposed operator of a matrix. Especially, the cross-CSD matrix of the array vector $\mathbf{u}(t)$ can be defined as

$$\mathbf{S}_{\mathbf{uu}}^{\alpha}(f)=\left\langle \mathbf{U}\left(f+\alpha/2\right)\mathbf{U}^{\mathrm{H}}(f-\alpha/2)\right\rangle_t, \tag{7}$$

where the diagonal matrix of $\mathbf{S}_{\mathbf{uu}}^{\alpha}(f)$ is called as the auto-CSD matrix.

2.2. Main properties of CSD

The time-delay property of CSD [14]: If $u(t)$ is a cyclostationary signal, whose CSD is $S_{uu}^{\alpha}(f)$, then the CSD of the signal $v(t)=u(t-t_0)$ can be expressed as

$$S_{vv}(f)=S_{uu}^{\alpha}(f)\mathrm{e}^{-\mathrm{j}2\pi\alpha t_0}. \tag{8}$$

Eq. (8) indicates that the CSD of a cyclostationary signal different from its PSD, is sensitive to the time-delay of the signal.

The filter property of CSD [14]: When the cyclostationary signal $u(t)$ undergoes a linear time-invariant transformation, and the output signal is $v(t)=\int_{-\infty}^{\infty}g(\tau)u(t-\tau)\,\mathrm{d}\tau$, then

$$S_{vv}^{\alpha}(f)=G(f+\alpha/2)S_{uu}^{\alpha}(f)G^{*}(f-\alpha/2), \tag{9}$$

$$S_{vu}^{\alpha}(f)=G(f+\alpha/2)S_{uu}^{\alpha}(f), \tag{10}$$

$$S_{uv}^{\alpha}(f)=S_{uu}^{\alpha}(f)G^{*}(f-\alpha/2), \tag{11}$$

where $G(f+\alpha/2)$ and $G(f-\alpha/2)$ are spectral components of transfer function $g(t)$ at frequencies $(f+\alpha/2)$ and $(f-\alpha/2)$, respectively. From Eqs. (9)–(11), the following expression can be

obtained:

$$S^{\alpha}_{vv}(f) = S^{\alpha}_{vu}(f)S^{\alpha}_{uv}(f)/S^{\alpha}_{uu}(f). \tag{12}$$

3. CYNAH theory of cyclostationary sound field

3.1. The scanning measurement technique

A microphone linear array is used here to measure the sound pressure signals scanning on the hologram plane, with a view to save channels. The signals scanning sampled are not temporal synchronous, so a reference microphone fixed near the sound source is necessarily used to reserve the phase information. Because of the time-delay property of CSD different from PSD, one new procedure different from the stationary NAH is proposed here to remove the influence of nonsynchronously measuring.

The scanning process on the hologram plane of the microphone array is shown in Fig. 1. In Fig. 1, $m = 1(1)M$ is the microphone in the array, $n = 1(1)N$ is the scanning step of the microphone array, Q is the number of gauging points on the hologram plane, and $Q = M \times N$. The nth scanning step begins at $t = \tau_n$ (potentially $\tau_1 = 0$), and then the sound pressure signals measured at the nth scanning step can be expressed as

$$\hat{\mathbf{p}}_n(t) = \left[p_{n1}(t-\tau_n), p_{n2}(t-\tau_n), \ldots, p_{nM}(t-\tau_n)\right]^{\mathrm{T}}, \tag{13}$$

where the superscript T is the transposed operator of a matrix, the superscript $\hat{}$ represents that the sound pressure signals are measured by scanning the microphone array step by step, which contains the time-delay information of scanning. The sound pressure measured by the reference microphone (called the reference pressure) at the nth scanning step can be expressed as $\hat{r}_n(t) = r(t-\tau_n)$.

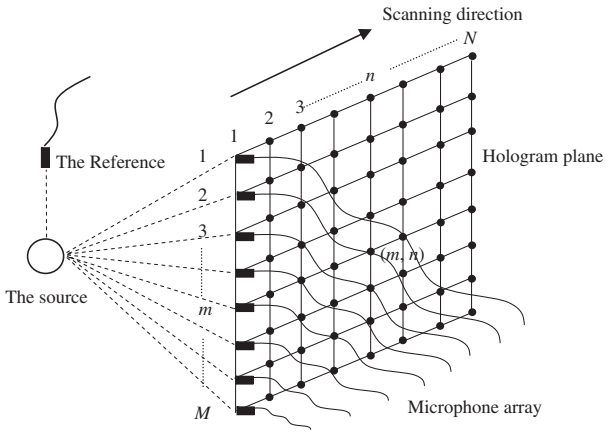

Fig. 1. The scanning process on the hologram plane of the linear microphone array.

According to time-delay property of CSD, a pair of cross-CSD matrixes of $\hat{\mathbf{p}}_n(t)$ and $\hat{r}_n(t)$, $\mathbf{S}^{\alpha}_{\hat{\mathbf{p}}_n\hat{r}_n}(f)$ and $\mathbf{S}^{\alpha}_{\hat{r}_n\hat{\mathbf{p}}_n}(f)$ can be expressed as follows:

$$\mathbf{S}^{\alpha}_{\hat{\mathbf{p}}_n\hat{r}_n}(f) = \mathbf{S}^{\alpha}_{\mathbf{p}_n r_n}(f)\mathrm{e}^{-\mathrm{j}2\pi\alpha\tau_n}, \tag{14}$$

$$\mathbf{S}^{\alpha}_{\hat{r}_n\hat{\mathbf{p}}_n}(f) = \mathbf{S}^{\alpha}_{r_n\mathbf{p}_n}(f)\mathrm{e}^{-\mathrm{j}2\pi\alpha\tau_n}, \tag{15}$$

where $\mathbf{S}^{\alpha}_{\mathbf{p}_n r_n}(f)$ and $\mathbf{S}^{\alpha}_{r_n\mathbf{p}_n}(f)$ are a pair of cross-CSD matrixes of the sound pressure on the M gauging points on the hologram plane and the reference pressure measured at the nth scanning step, after the influence of the time-delay τ_n is removed.

The cyclic time-delay factor $\mathrm{e}^{-\mathrm{j}2\pi\alpha\tau_n}$ can be calculated as follows:

$$\mathrm{e}^{-\mathrm{j}2\pi\alpha\tau_n} = S^{\alpha}_{\hat{r}_n\hat{r}_n}(f)/S^{\alpha}_{\hat{r}_1\hat{r}_1}(f), \tag{16}$$

where $S^{\alpha}_{\hat{r}_n\hat{r}_n}(f)$ is the CSD of $\hat{r}_n(t)$, and $S^{\alpha}_{\hat{r}_1\hat{r}_1}(f)$ is the CSD of $\hat{r}_1(t)$.

Substituting Eq. (16) into Eqs. (14)–(15), $\mathbf{S}^{\alpha}_{\mathbf{p}_n r_n}(f)$ and $\mathbf{S}^{\alpha}_{r_n\mathbf{p}_n}(f)$ can be expressed as follows:

$$\mathbf{S}^{\alpha}_{\mathbf{p}_n r_n}(f) = \mathbf{S}^{\alpha}_{\hat{\mathbf{p}}_n\hat{r}_n}(f)S^{\alpha}_{\hat{r}_1\hat{r}_1}(f)/S^{\alpha}_{\hat{r}_n\hat{r}_n}(f), \tag{17}$$

$$\mathbf{S}^{\alpha}_{r_n\mathbf{p}_n}(f) = \mathbf{S}^{\alpha}_{\hat{r}_n\hat{\mathbf{p}}_n}(f)S^{\alpha}_{\hat{r}_1\hat{r}_1}(f)/S^{\alpha}_{\hat{r}_n\hat{r}_n}(f). \tag{18}$$

Finally, a pair of cross-CSD matrixes of the sound pressure on the hologram plane and the reference pressure after removing the influence of time-delay of scanning measurement, $(\mathbf{S}^{\alpha}_{\mathbf{p}r}(f))_{Q\times 1}$ and $(\mathbf{S}^{\alpha}_{r\mathbf{p}}(f))_{1\times Q}$ can be expressed as follows:

$$\left(\mathbf{S}^{\alpha}_{\mathbf{p}r}(f)\right)_{Q\times 1} = \left[\left(\mathbf{S}^{\alpha}_{\mathbf{p}_1 r_1}(f)\right)^{\mathrm{T}}, \left(\mathbf{S}^{\alpha}_{\mathbf{p}_2 r_2}(f)\right)^{\mathrm{T}}, \ldots, \left(\mathbf{S}^{\alpha}_{\mathbf{p}_n r_n}(f)\right)^{\mathrm{T}}, \ldots, \left(\mathbf{S}^{\alpha}_{\mathbf{p}_N r_N}(f)\right)^{\mathrm{T}}\right]^{\mathrm{T}}, \tag{19}$$

$$\left(\mathbf{S}^{\alpha}_{r\mathbf{p}}(f)\right)_{1\times Q} = \left[\mathbf{S}^{\alpha}_{r_1\mathbf{p}_1}(f), \mathbf{S}^{\alpha}_{r_2\mathbf{p}_2}(f), \ldots, \mathbf{S}^{\alpha}_{r_n\mathbf{p}_n}(f), \ldots, \mathbf{S}^{\alpha}_{r_N\mathbf{p}_N}(f)\right]. \tag{20}$$

According to the filter property of CSD, the following relationship can be proved:

$$\left(\mathbf{S}^{\alpha}_{\mathbf{pp}}(f)\right)_{Q\times 1} = \mathrm{diag}\left(\left(\mathbf{S}^{\alpha}_{\mathbf{pp}}(f)\right)_{Q\times Q}\right) = \mathrm{diag}\left(\left(\mathbf{S}^{\alpha}_{\mathbf{p}r}(f)\right)_{Q\times 1}\left(\mathbf{S}^{\alpha}_{r\mathbf{p}}(f)\right)_{1\times Q}/S^{\alpha}_{rr}(f)\right) \tag{21}$$

where $(\mathbf{S}^{\alpha}_{\mathbf{pp}}(f))_{Q\times Q}$ is the cross-CSD matrix of the sound pressure on the hologram plane, $(\mathbf{S}^{\alpha}_{\mathbf{pp}}(f))_{Q\times 1}$ is the auto-CSD matrix, and diag($\cdot$) is diagonal operator of a matrix. The relationship between the sound pressure on the hologram gauging points and the reference pressure is obtained by Eq. (21), and a similar relationship can be obtained for the reconstruction plane.

3.2. The reconstruction of cyclostationary sound field

Both of the hologram and reconstruction surfaces are assumed as planar, shown in Fig. 2. The hologram plane S_h locates at $z = z_h$, and the reconstruction plane S_c locates at $z = z_c$. Symbolically, $\lfloor S^{\alpha}_{pp}(x, y, z_h, f)\rfloor_{Q\times 1}$ is the auto-CSD matrix of the sound pressure on the hologram grids, $\lfloor S^{\alpha}_{pp}(x, y, z_c, f)\rfloor_{Q\times 1}$ is the auto-CSD matrix of the sound pressure on the reconstruction grids, $S^{\alpha}_{rr}(f)$ is the CSD of the reference pressure, and $\lfloor S^{\alpha}_{pr}(x, y, z_h, f)\rfloor_{Q\times 1}$ are a pair of cross-CSD matrixes between the sound pressure on the hologram grids and the reference pressure,

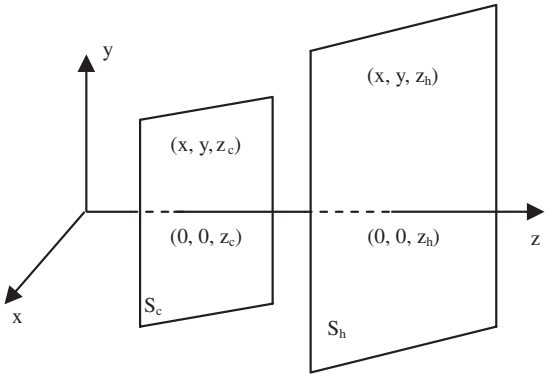

Fig. 2. The sketch map of sound field propagation.

$\lfloor S^{\alpha}_{rp}(x,y,z_c,f)\rfloor_{1\times Q}$ and $\lfloor S^{\alpha}_{pr}(x,y,z_c,f)\rfloor_{Q\times 1}$ are a pair of cross-CSD matrixes between the sound pressure on the reconstruction grids and the reference pressure. The coordinates are contained in above symbols in order to describe the CYNAH procedure conveniently.

$\lfloor S^{\alpha}_{rp}(x,y,z_h,f)\rfloor_{1\times Q}$ and $\lfloor S^{\alpha}_{pr}(x,y,z_h,f)\rfloor_{Q\times 1}$ can be calculated by Eqs. (19–20) from the sound pressure on the hologram gauging points scanning measured step by step, then $\lfloor S^{\alpha}_{pp}(x,y,z_h,f)\rfloor_{Q\times 1}$ can be calculated by Eq. (21). It is impossible to reconstruct $\lfloor S^{\alpha}_{pp}(x,y,z_c,f)\rfloor_{Q\times 1}$ from $\lfloor S^{\alpha}_{pp}(x,y,z_h,f)\rfloor_{Q\times 1}$ directly due to the loss of phase information. However, $\lfloor S^{\alpha}_{rp}(x,y,z_h,f)\rfloor_{1\times Q}$ and $\lfloor S^{\alpha}_{pr}(x,y,z_h,f)\rfloor_{Q\times 1}$ still reserve the phase information and can be used directly to reconstruct sound field.

It is assumed that $[p(x,y,z_h,f)]_{Q\times 1}$ and $r(f)$ are the spectral functions of sound pressure on the hologram plane and the reference pressure, respectively, $\lfloor S^{\alpha}_{rp}(x,y,z_h,f)\rfloor_{1\times Q}$ depends on the function of $r(f+\alpha/2)$ and $[p(x,y,z_h,f-\alpha/2)]^H$, while $\lfloor S^{\alpha}_{pr}(x,y,z_h,f)\rfloor_{Q\times 1}$ depends on the function of $[p(x,y,z_h,f+\alpha/2)]$ and $r^*(f-\alpha/2)$. Therefore, $\lfloor S^{\alpha}_{rp}(x,y,z_c,f)\rfloor_{1\times Q}$ and $\lfloor S^{\alpha}_{pr}(x,y,z_c,f)\rfloor_{Q\times 1}$ should be reconstructed at frequencies $(f-\alpha/2)$ and $(f+\alpha/2)$, respectively, from $\lfloor S^{\alpha}_{rp}(x,y,z_h,f)\rfloor_{1\times Q}$ and $\lfloor S^{\alpha}_{pr}(x,y,z_h,f)\rfloor_{Q\times 1}$. In this way, the CYNAH reconstruction relationship can be expressed as follows:

$$S^{\alpha}_{rp}(x,y,z_c,f)=F^{-1}\left[\tilde{S}^{\alpha}_{rp}(k_x,k_y,z_h,f)\tilde{G}^{-1}_{Drp}(k_x,k_y,z_h-z_c)\right], \tag{22}$$

$$S^{\alpha}_{pr}(x,y,z_c,f)=F^{-1}\left[\tilde{S}^{\alpha}_{pr}(k_x,k_y,z_h,f)\tilde{G}^{-1}_{Dpr}(k_x,k_y,z_h-z_c)\right]. \tag{23}$$

In Eqs. (22)–(23):

$$\tilde{S}^{\alpha}_{rp}(k_x,k_y,z_h,f)=F\left[S^{\alpha}_{rp}(x,y,z_h,f)\right]\ ,\ \ \tilde{S}^{\alpha}_{pr}(k_x,k_y,z_h,f)=F\left[S^{\alpha}_{pr}(x,y,z_h,f)\right],$$

$$\tilde{G}_{Drp}(k_x,k_y,z_h-z_c)=\begin{cases}\exp\left[\mathrm{j}(z_h-z_c)\sqrt{k_{rp}^2-k_x^2-k_y^2}\right], & k_x^2+k_y^2\leqslant k_{rp}^2,\\ \exp\left[-(z_h-z_c)\sqrt{k_x^2+k_y^2-k_{rp}^2}\right], & k_x^2+k_y^2>k_{rp}^2,\end{cases}$$

$$\tilde{G}_{Dpr}(k_x, k_y, z_h - z_c) = \begin{cases} \exp\left[\mathrm{j}(z_h - z_c)\sqrt{k_{pr}^2 - k_x^2 - k_y^2}\right], & k_x^2 + k_y^2 \leqslant k_{pr}^2, \\ \exp\left[-(z_h - z_c)\sqrt{k_x^2 + k_y^2 - k_{pr}^2}\right], & k_x^2 + k_y^2 > k_{pr}^2, \end{cases}$$

$$k_{rp} = 2\pi(f - \alpha/2)/c, \quad k_{pr} = 2\pi(f + \alpha/2)/c,$$

where c is the sound speed. $\lfloor S_{rp}^{\alpha}(x, y, z_c, f)\rfloor_{1\times Q}$ and $\lfloor S_{pr}^{\alpha}(x, y, z_c, f)\rfloor_{Q\times 1}$ can be calculated by Eqs. (22)–(23). Then, $\lfloor S_{pp}^{\alpha}(x, y, z_c, f)\rfloor_{Q\times 1}$ can be obtained from Eq. (21).

The CYNAH can be implemented with the following procedure:

(1) To compute the three-dimensional CSD figure of the reference pressure, which is the function of frequency and cyclic frequency.
(2) To find out all candidate cyclic frequencies from the CSD figure of the reference pressure.
(3) To estimate the real cyclic frequencies from those candidate cyclic frequencies. In some applications, the cyclic frequencies may not be known in advance. Some works have been developed to estimate the cyclic frequencies of the nth order cyclostationary signal [15,16].
(4) To select the appropriate cyclic frequencies from those estimated cyclic frequencies. Even if all the cyclic frequencies of signals have been obtained, some appropriate cyclic frequencies should be selected carefully from all ones in order to obtain the interested information. There is no universal method in selecting the appropriate cyclic frequencies yet, and prior information is absolutely necessary. Some works [9–13] involve how to select appropriate cyclic frequencies from the vibratory or acoustic signals of rotating machineries, according to the rotation speed, the type of faults, and the feature frequencies of the faults, etc. The appropriate cyclic frequency is assumed known here in advance in order to focus on the reconstruction of cyclostationary sound field.
(5) To reconstruct the CSD distribution of sound pressure on the reconstruction plane by Eqs. (21)–(23) at the selected cyclic frequencies.

Note that the CSD will be simplified to the PSD when $\alpha = 0$, thus, the CYNAH technique reduces to the NAH technique.

4. Numerical simulations

4.1. Simulation signals

One signal is employed to simulate unity velocities on a square piston in an infinite and rigid baffle that are considered as one sound source Ω, and it is expressed by

$$V(t) = (a(t))\cos\left(2\pi f_a t\right), \tag{24}$$

where $a(t)$ is a purely stationary random noise with zero mean and $f_a = 300$ Hz. The velocity signal is a cyclostationary amplitude-modulation (AM) signal with the unique cyclic frequency 600 Hz [14], $\cos(2\pi f_a t)$ is the carrier wave function, and $a(t)$ is its modulating function. The PSD of $a(t)$ and $V(t)$ are shown in Figs. 3(a) and (b). It can be found from Figs. 3(a) and (b) that the

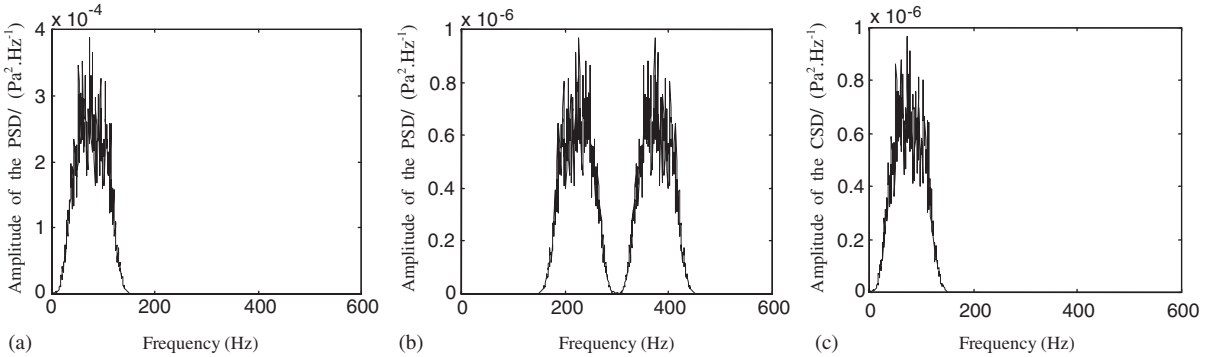

Fig. 3. The analysis of the simulation velocity signal: (a) The PSD of modulating components of the velocity signal. (b) The PSD of the velocity signal. (c) The CSD of the velocity signal when $\alpha = 600$ Hz.

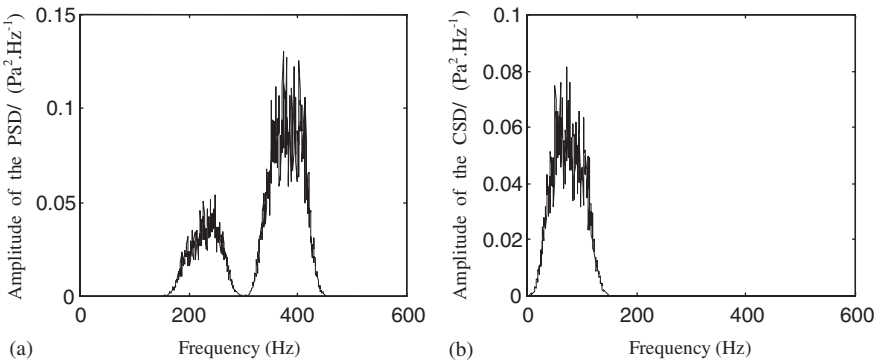

Fig. 4. The analysis of the simulation sound signal: (a) The PSD of the sound signal. (b) The CSD of the sound signal when $\alpha = 600$ Hz.

spectra of $a(t)$ and the carrier wave are mixed up in PSD of $V(t)$ with the influence of modulation, and the spectrum of $a(t)$ becomes two sidebands around f_a. The CSD of $V(t)$ when $\alpha = 600$ Hz is shown in Fig. 3(c), where the disturbance of the carrier wave is removed, and the spectral characteristics of the modulating wave function $a(t)$ are shown clearly.

The dimensions of the piston are assumed as $0.3 \times 0.3\,\mathrm{m}^2$, and the source is located at the median of the hologram plane, whose center is (0,0,0). The linear array consisted of 25 microphones scans on the hologram plane step by step, and the number of scanning steps is 25. The distance from the hologram plane S_h to the source plane is $d_h = 0.08$ m, and the distances between adjoining points in x and y directions are $\Delta x = \Delta y = 0.08$ m.

The sound pressure can be determined by the second Rayleigh's integral formulation. The PSD of the sound pressure radiated from the source is shown in Fig. 4(a), which is different from the PSD of $V(t)$ in Fig. 3(b) because of the influence of the piston. However, the sound pressure is still cyclostationary. The CSD of the sound pressure when $\alpha = 600$ Hz is shown in Fig. 4(b), and the spectral characteristics of the modulating components are shown clearly.

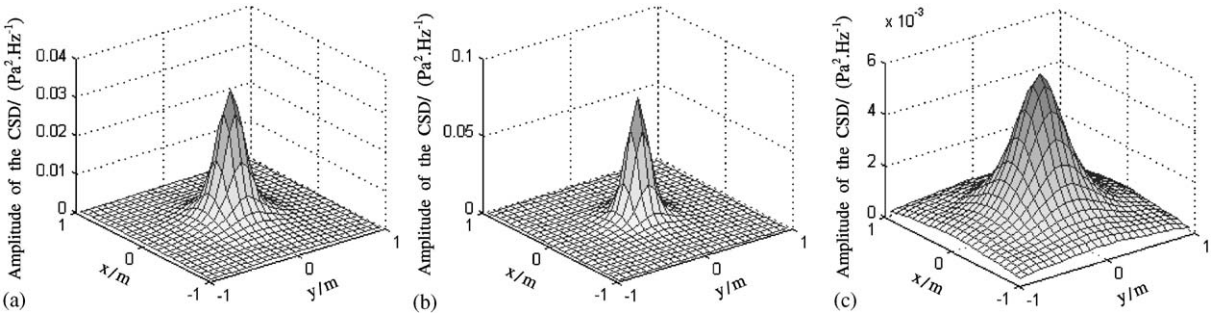

Fig. 5. The CYNAH reconstruction of sound field in the simulation when $f = 90\,\text{Hz}$, $\alpha = 600\,\text{Hz}$: (a) The CSD distribution on the hologram plane $z_h = 0.08\,\text{m}$. (b) The CSD distribution on the reconstruction plane $z = 0\,\text{m}$. (c) The CSD distribution on the reconstruction plane $z = 0.3\,\text{m}$.

4.2. The CYNAH reconstruction of sound field

It is assumed that the reference locates at (0,0,0.05) m. The reconstructed cyclic frequency and frequency are selected to be $\alpha = 600\,\text{Hz}$, and $f = 90\,\text{Hz}$, respectively. The CSD distributions of sound pressure on the hologram plane and two reconstruction planes are shown in Figs. 5(a)–(c), respectively. The errors of reconstruction in Figs. 5(b) and (c) are 7.53%, and 3.71% respectively, calculated by means of $100^*\|\mathbf{S} - \mathbf{S}_{ex}\|/\|\mathbf{S}_{ex}\|$, where $\|\bullet\|$ is the L2 norm, $\mathbf{S}$ is the reconstructed result, and $\mathbf{S}_{ex}$ is the CSD of real sound pressure on reconstruction plane. The errors are a bit because no any disturbances are involved, such as noise contamination, the departure of microphones, and the phase discrepancy of microphones, etc.

The contamination of noise is considered here. It is assumed that the disturbed noise is stationary random white-noise independent of the sources, and it is equally distributed over the sound field. The sound levels of noise are assumed to be 11.65 dB lower than the levels of the sound pressure of the hologram grid where the sound pressure is maximal. The errors of reconstruction in Figs. 5(b) and (c) increases to 8.62% and 7.49%, respectively.

5. The experiment of CYNAH

5.1. The experimental equipment

The experiment is implemented in an anechoic-chamber to validate the CYNAH procedure. The sound pressure radiated from an alternating motor is cyclostationary, which is used as the sound source. The linear array consisting of 24 microphones is installed on a frame which can be moved in an overall hologram plane step-by-step and the number of scanning steps is 24. Another microphone as a reference is set near the motor. The distance from the holography plane S_h to the source is $d_h = 0.05\,\text{m}$, and the distances between adjoining points in x and y directions are $\Delta x = \Delta y = 0.045\,\text{m}$. A record system with 32 channels is used for synchronous sampling signals from the microphone array and the reference, and the photos of some equipment are shown in Figs. 6(a) and (b).

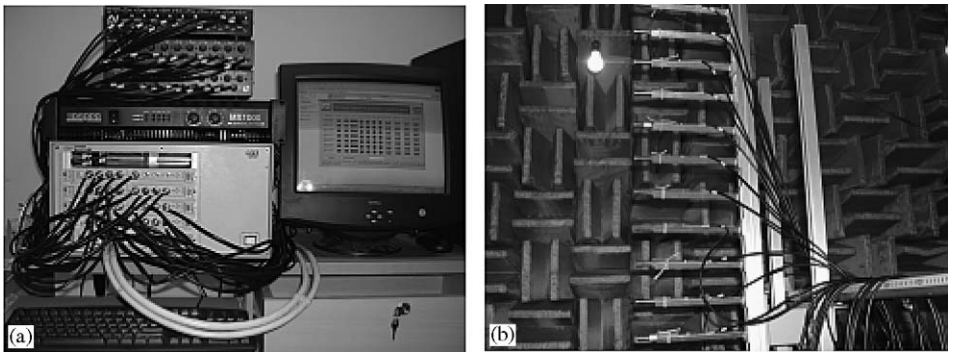

Fig. 6. The experimental equipment: (a) The record system, used to record synchronously data from microphone array and the reference microphone. (b) The microphone array, used to sample sound pressure on hologram.

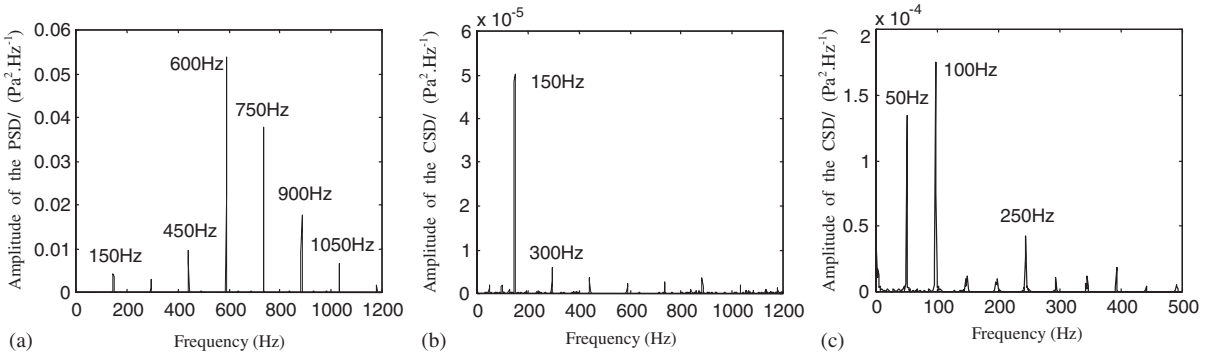

Fig. 7. The analysis of the sound signal of the motor: (a) The PSD of the sound signal. (b) The CSD of the sound signal when $\alpha = 1474$ Hz. (c) The CSD of the sound signal when $\alpha = 1280$ Hz.

5.2. The CYNAH sound field reconstruction

The cyclic frequencies are selected as 1280 and 1474 Hz, according to the CYNAH procedure in Section 3.2. The PSD of the sound pressure radiated from the motor is shown in Fig. 7(a), and the CSD when $\alpha = 1474$ and 1280 Hz are shown in Figs. 7(b) and (c), respectively. It can be found in Fig. 7(a) that the fundamental frequency is 150 Hz, and other frequencies are all its multiples. The information of fundamental frequency is not easily found in Fig. 7(a) because its power is much smaller than other frequency components. In Fig. 7(b), the fundamental frequency is shown very clearly because other components are all suppressed. In Fig. 7(c), the information of the shaft frequency 50 Hz can be found, which do not appear in the PSD of Fig. 7(a). Consequently, the CYNAH hologram can display apparently radiated sound power of the motor at fundamental frequency 150 Hz and shaft frequency 50 Hz. Here, only the CSD results at 150 Hz on the hologram and two reconstruction planes are provided in Figs. 8(a)–(c) respectively.

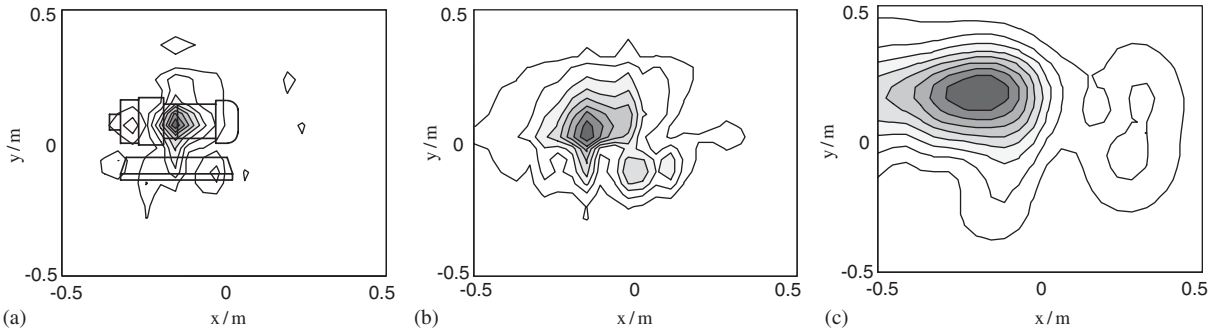

Fig. 8. The CYNAH reconstruction of sound field radiated from the motor when $f = 150\,\text{Hz}$, $\alpha = 1474\,\text{Hz}$: (a) The CSD distribution on the hologram plane $z_h = 0.05\,\text{m}$. (b) The CSD distribution on the reconstructed plane $z = 0\,\text{m}$. (c) The CSD distribution on the reconstructed plane $z = 0.3\,\text{m}$.

6. Conclusions

The CYNAH procedure is proposed here for analyzing cyclostationary sound field, and the CSD of sound pressure is shown by the CYNAH hologram, instead of the PSD or spectrum. Some drawbacks resulting from NAH of cyclostationary sound field can be overcome, such as sidebands disturbance, the loss of time-varying statistics, etc. The simulation and experimental instances show that the modulation mechanism present in the vibratory response of rotating machineries can be obtained by CYNAH more clearly than NAH. Only the CYNAH theory and its some simple instances are introduced here yet, and more applications in analyzing sound field radiated from practical rotating machineries, such as the gear, or rolling-element bearing, should be further researched.

Acknowledgements

This work is aided by the Natural Science Fund of China (No. 10474065).

References

[1] E.G. Williarms, J.D. Maynard, E. Skudrzyk, Sound source reconstructions using a microphone array, *Journal of the Acoustical Society of America* 68 (1980) 340–344.
[2] B.G. Kevin, J. Hald, STSF-practical instrumentation and applications, *B&K Technical Review* 2 (1989) 1–27.
[3] T. Loyan, J.C. Pascal, P. Gsillard, Broadband acoustic holography reconstruction from acoustic intensity measurements. I: Principle of the method, *Journal of the Acoustical Society of America* 84 (1988) 1744–1750.
[4] M.R.S. Bai, Application of BEM (boundary element method)-based acoustic holography to radiation analysis of sound sources with arbitrarily shaped geometries, *Journal of the Acoustical Society of America* 92 (1992) 533–549.
[5] J.A. Mann, J.C. Pascal, Locating noise source on an industrial air compressor using broadband acoustical holography from intensity measurements (BAHIM), *Noise Control Engineering Journal* 39 (1992) 3–12.

[6] E.G. Williams, et al., Interior near-field acoustical holography in flight, *Journal of the Acoustical Society of America* 108 (2000) 1451–1463.
[7] J. Hald, Time domain acoustical holography and its applications, *Sound and Vibration* 2 (2001) 16–25.
[8] T. Tanaka, et al., Tire noise analysis during vehicle acceleration running with acoustical holography, *Transactions of the Japan Society of Mechanical Engineers, Part C* 69 (2003) 959–965.
[9] A.C. Mccormick, A.K. Nandi, Cyclostationarity in rotating machine vibrations, *Mechanical Systems and Signal Processing* 12 (1998) 225–242.
[10] C. Capdessus, M. Sidahmed, J.L. Lacoume, Cyclostationary processes: Application in gear faults early diagnosis, *Mechanical Systems and Signal Processing* 14 (2000) 371–385.
[11] I. Antoniadis, G. Glossiotis, Cyclostationary analysis of rolling-element bearing vibration signals, *Journal of Sound and Vibration* 248 (2001) 829–845.
[12] J. Antoni, R.B. Randall, Differential diagnosis of gear and bearing faults, *Journal of Vibration and Acoustics, Transactions of the ASME* 124 (2002) 165–171.
[13] J. Antoni, F. Bonnardot, A. Raad, M.E. Badaoui, Cyclostationary modelling of rotating machine vibration signals, *Mechanical Systems and Signal Processing* 18 (2004) 1285–1314.
[14] W.A. Gardner, Exploitation of spectral redundancy in cyclostationary signals, *IEEE Signal Processing Magazine* 8 (1991) 14–36.
[15] A.V. Dandawate, G.B. Giannakis, Statistical tests for presence of cyclostationarity, *IEEE Transaction on Signal Processing* 42 (1994) 2355–2369.
[16] G.K. Yeung, W.A. Gardner, Search efficient methods of detection of cyclostationary signals, *IEEE Transactions on Signal Processing* 44 (1996) 1214–1223.